Energy & Environmental Science

Accepted Manuscript

This article can be cited before page numbers have been issued, to do this please use: N. Cui, C. Dai, J. Liu, L. Gu, R. Ge, T. Du, Z. Wang and Y. Qin, *Energy Environ. Sci.*, 2020, DOI: 10.1039/D0EE00922A.

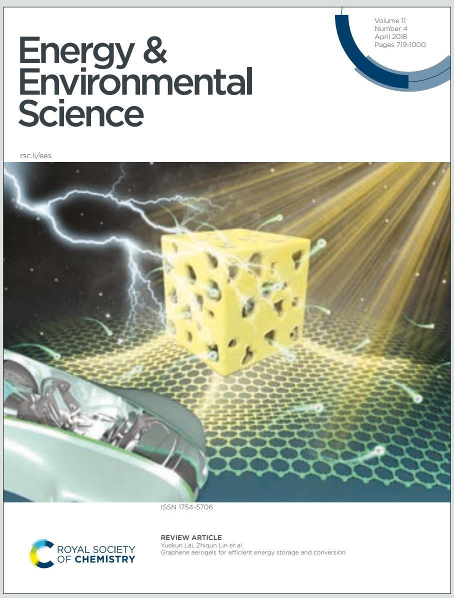

View Article Online
DOI: 10.1039/D0EE00922A

COMMUNICATION

Received 00th January 20xx,
Accepted 00th January 20xx

DOI: 10.1039/x0xx00000x

Increasing the output charge quantity of triboelectric nanogenerator through frequency-multiplying with multi-gap structure friction layer

Nuanyang Cui,[a] Cuihua Dai,[a] Jinmei Liu,[a] Long Gu,[a] Rui Ge,[a] Tao Du,[a] Zheng Wang,[a] and Yong Qin[b*]

Because the output current of a TENG is mainly determined by the quantity of triboelectric charge carried on the friction layer. The triboelectric charge capacity and the charge driving ability of the friction layer are the key parameters for enhancing the output performance of Triboelectric Nanogenerator (TENG). In this paper, we developed a new TENG with a multi-gap structure friction layer. The presence of these gaps create more contacts between the friction layers, which will produce much more separated triboelectric charges and more output charge quantity. Besides, these gaps also make the TENG to generate more output current pulses in each driven cycle, which means that the frequency of the output current will be several times the driven frequency. In one driven cycle, a general TENG without gaps in friction layer generates 2 current pulses and output 0.23 nC/cm² unit area charge quantity, while a TENG with seven gaps in the friction layer generates about 14 current output pulses and output 294 nC/cm² unit area charge quantity, which is 1.18 times the value of the record one. This work will contribute to the rapid increase of TENG's performance and speed up its applications.

Key words: TENG; Frequency Multiplication; Output Charge Quantity; Unit area charge quantity per cycle (UCQC); Multi-Gap

Introduction

With the development of sensors in the past several decades, the large scale sensor networks such as Internet of Things bring the convenience to our lives, but how to power the widespread sensors has been the great bottle neck to limit their applications [1, 2]. The traditional power sources, such as transmission network or chemical batteries, could not sufficiently adapt to the distributed and miniaturized sensors or other functional electronics that request some more reliable sources of distributed and sustainable energy. Triboelectric Nanogenerator (TENG) that can harvest the mechanical energy in the ambient environment has the potential to be an ideal power source for the small electronics. Since it was invented in 2012, TENG has attracted lots of attentions for its tremendous application potential as a sustainable power source[3-8], and has been demonstrated to scavenge various kinds of mechanical energy from the environment successfully, such as sound wave[9-12], ambient vibration[13-16], body motion[17-21], air flow[22-24], etc. And many efforts have been paid to improving the output performance of the TENG. At present, there are mainly two kinds of approaches to maximize the power supply function of TENG. One is the external impedance matching approach [25-29]. The other one is enhancing the output performance of TENG itself [21, 30-34], which is more fundamental for the applications of TENG.

In the respect of enhancing the output performance, the TENG has experienced a huge development. From choosing the different materials, designing the new device structure to constructing nano-structure and other surface modification technique, different methods have been developed to increase the performance of TENG step by step. And almost all these efforts are for the purpose of effectively increasing the charge density of the TENG's friction layer. The fundamental reason is because that the charge output capability is positively correlated with surface charge density of frictional layer and output current frequency. The more electrostatic charges exist in the friction layer the more induced charges will move in the external circuit. In fact, different

[a.] School of Advanced Materials and Nanotechnology, Xidian University,710071, China
[b.] Institute of Nanoscience and Nanotechnology, Lanzhou University, 730000, China
* To whom correspondence should be addressed: qinyong@lzu.edu.cn
†Electronic Supplementary Information (ESI) available: [details of any supplementary information available should be included here]. See DOI: 10.1039/x0xx00000x

View Article Online
DOI: 10.1039/D0EE00922A

optimizations, charge density enhancement, external load matching and rarely mentioned output frequency increment, do not conflict with each other in theory and can be applied in a TENG device at the same time. Similarly, the more output current frequency also contributes the more charges flow in external circuit. Generally, it is considered that the output current frequency of TENG is equal to the driven frequency which depends on the driving mode. However, if the output frequency can be increased under the same driving mode, it is possible to further improve the output performance of TENG.

In this work, a new kind of frequency-multiplied TENG with multi-gap friction layer (FTNG) is developed to produce much more separated triboelectric charges and more output pulse, and further enhance the unit area charge quantity per cycle (UCQC) of TENG. The gaps created in the friction layer can provide more chances for the materials with different electronegativity to contact each other in one driven cycle. A FTNG with 3 gaps in the negative layer generates 6 current pulses in one cycle and gives an UCQC of 15.6 nC/cm^2, while a general compared TENG with no gaps in friction layer only generates 2 pulses in one cycle and gives a small UCQC of 0.23 nC/cm^2. Another FTNG with seven gaps and without surface micro-structure outputs a UCQC of 47 nC/cm^2. But, when the FTNG with seven gaps is modified with micro-structure on its friction layers' surface, it generates two broadened wave packets and a large UCQC of 294 nC/cm^2 that is 1.18 times of the record one[35].

Result and discussion

The structure of the FTNG is schematically shown in Fig. 1a. Like a general TENG, there are two major parts in this device. The lower part is a multi-gap part. It consists of a piece of PVDF thin film, a piece of Nylon thin film, Al (aluminium) electrode and spacers used to create gaps between the films and electrode. The upper part is Al plate, which acts as the part of positive electrode and positive friction layer. The basic working mechanism of FTNG for harvesting mechanical energy is shown in Fig. 1b. It is based on the vertical contact-separation mode. In the driven process, the upper small Al electrode contacts and separates with the multi-gap lower part periodically. The in-between PVDF and Nylon thin films will be clamped and released periodically, and the positive and negative triboelectric charges will be accumulated on the Nylon and PVDF films respectively.

As shown in Fig. 1b, when the upper Al plate moves to the PVDF film, from Stage Ⅰ to Stage Ⅱ, the electrons in the external circuit will be repelled to the bottom Al electrode by the negative charges on the PVDF film. The current flow from the bottom Al electrode to the top Al electrode. When the top Al electrode move to the Nylon film, from Stage Ⅱ to Stage Ⅲ, some of the electrons in the external circuit will flow to the top Al electrode under the influence of the positive charges on the Nylon film. The current flows from the top Al electrode to the bottom Al electrode. And then, until to Stage Ⅴ, although the muti-gap structure is continuously pressed and gradually released, i.e. the PVDF film, Nylon film and bottom Al electrode first contact and then separate with each other, there is no current flowing in the external circuit during this time. When the top Al electrode moves to the position in Stage Ⅵ, the current will flow from the lower Al electrode to the upper Al electrode. This is the reverse process of Stage Ⅱ to Stage Ⅲ. At last, when the upper Al plate moves to the initial position in Stage Ⅰ, the external current will flow to the bottom Al electrode again. So, in one cycle, there will appear 4 current flows in the external circuit and 3 contacts between the different layers with different electronegativity materials. The 3 contacts appear in Stage Ⅱ, Stage Ⅲ and Stage Ⅳ. Compare with the FTNG, a general TENG has only 2 current flows and 1 contact between the friction layers in one cycle. More contacts and more current flows must bring more triboelectric charge separations and large UCQC of TENG.

The first FTNG was fabricated according to the schematic in Fig. 1a. The area of the lower multi-gap part is 2 cm×2 cm, the area of the upper Al electrodes is 1 cm×1 cm, the thicknesses of PVDF film and Nylon film are both 5 µm and the height of the gaps is 180 µm. Driven by a linear motor, the FTNG works continuously for 15 minutes. The short circuit current is shown in Fig. 1c. Like a general TENG's performance, it also shows a gradual charge accumulation process. In Fig. 1d, the front red dashed box shows the first five cycles of output current at the beginning of Fig. 1c. In the third cycle the third pulse appears. It comes from the process of Stage Ⅳ to Stage Ⅴ, as shown in Fig. 1b. In the fourth cycle the last current pulse appears. It comes from the process of Stage Ⅱ to Stage Ⅲ. And the purple dashed box, which is a large version of the end of Fig. 1c, shows one cycle of the stable output current. It appears visible 4 pulses in one cycle. By integrating the current, the charge quantity transferred by each pulse can be calculated. They are 3.7 nC, 0.9 nC, 0.71 nC and 3.2 nC respectively. The second and third pulses' charge, which comes from the relative movement of Nylon film, is obviously smaller than the others' charge quantity. This is because Nylon is so close to Al in the triboelectric series and cannot separate more triboelectric charges. So, the accumulated charge in Nylon film is much less than that in PVDF film, and the influence of Nylon film on the output current is also less than that of PVDF film. The open-circuit voltage of this FTNG is shown in Figure S1, its peak value reaches 60 V. In this work, the current signal and voltage signal were measured through Stanford Research Systems (low-noise preamplifier SR560 and low-noise current preamplifier SR570). The input resistances of the preamplifiers were 100 MΩ and 10 kΩ, respectively.

To further analyse the performance of FTNG, three comparing TENGs are prepared: TENG A is a general TENG with the friction layer consisting of three pieces of polymer film, PVDF, Nylon and PVDF, and no gaps between them; TENG B is a FTNG with the friction layer consisting of PVDF film, Nylon film and PVDF film, and the height of the gaps between these films is 180 µm; TENG C is anther FTNG with the same multi-gap structure friction layer like that in TENG B, but the order of films is Nylon, PVDF and Nylon. After working for 15 minutes under the same driving condition, the currents of these three devices are measured and shown in Fig. 2. For the general TENG A, there are two current pulses in one cycle, and the charge quantity per

View Article Online
DOI: 10.1039/D0EE00923A

cycle (CQC) is only 0.23 nC. The output is very small because no structure optimization is made on TENG A. For the TENG B, there are three current pulses in each half cycle. The second pulse, which is marked by a red point as shown in Fig. 2b, is very small. That is due to the weak charge capacity of Nylon. When we put the PVDF layer in the middle layer, the second current pulse stands out clearly in each half cycle, as shown in Fig. 2c. At last, the output charges in one cycle are calculated: 21.5 nC for TENG B and 15.8 nC for TENG C. They are both much better than the 0.23 nC of general TENG A without gap structure. The FTNG with multi-gaps (TENG C) exhibits the best performance.

From above results, it can be seen that the introduction of the gaps greatly enhances the performance of TENG. To investigate the effect of the multi-gap structure in depth, we prepared a group of new FTNGs with two gaps in the friction layer and the gap heights h of these devices are 180 μm, 310 μm, 440 μm, 570 μm respectively. Working under the same condition for 15 minutes, these four FTNGs' outputs become stable. The output currents are shown in Fig. 3a-d. The output current and output charge increase obviously along with the rise of width of gaps. However, through the theoretic calculation, it is found that the output charge is almost irrelevant to the width of gaps. As shown in Fig. 3e, when the height of gaps is h, the charge accumulated on the PVDF and Nylon is $-Q$ and Q, and the distance between PVDF film and the top Al electrode is d, the induced charge Q' on the Al electrode can be calculated as $2Qh/(4h+2d)$. The derivation process is given in supporting information. According to this result, when the top Al electrode is far enough away from PVDF, Q' tends to 0, and when the Al electrode is close to the PVDF film, Q' tends to $Q/2$, as shown in Fig. 3f. So, when the top Al electrode move to the PVDF film, the positive charges flows in the external circuit is $Q/2$. It is irrelevant to the height h. The reason leading to deviation between calculated and measured results is the bend of PVDF and Nylon films. As shown in Fig. S3, when the positive and negative charges are accumulated on Nylon and PVDF films, these two films will attract each other under the electric field force. The centre areas of the films will attach tightly to each other, and the effective interstitial area will be reduced. At last, along with the increase of the gaps' height, the effective interstitial area of the films recovered, and the output charge quantity increases also.

Increasing the height and number of gaps is very beneficial for the enhancement of FTNG's output performance. However, this enhancement of output performance is not monotonically with them. The output of FENG cannot be increased infinitely by increasing the height and the number of the gaps. A FTNG with five 570 μm high gaps is prepared. Its output current is shown in Fig. 4a. Compared with the results in Fig. 3, the peak value of this current is not exactly small, but its peak curve is much sharper. And the CQC of this five-gap FTNG is only 14 nC. It is found that when the total height of the multi-gap layer is too large, larger than about 1.5 mm, the air discharge will appear in the gaps frequently. That will reduce the accumulated charge on the polymer films. In fact, the biggest current peak in Fig. 4a is not an induced current pulse but an air discharge peak. In the zoomed-in figure framed with the red dashed box, a sharp turning point is marked by a red arrow. At this point an air discharge occurred. To control the total height, a new FTNG is prepared with seven 180 μm high gaps. Due to the total height is less than 1.5 mm, there is no air discharge in the gaps. The output current is shown in Fig. 4b, it can be calculated that the UCQC reaches 47 nC/cm^2.

Fundamentally, the frequency-multiplying technique with multi-gap structure friction layer is an effective structure design method to enhance the output performance of TENG, and not conflict with other enhancement methods such as surface optimization or external load matching. So, to further enhance the output performance of TENG combined with other techniques, a new FTNG with seven 180 μm high gaps and the PVDF and Nylon films with surface modified micro-structure as the friction layers is designed and developed. The optical micrograph of the micro-structure is shown in the inset of Fig. 4c. And the UCQC of this FTNG reaches 98 nC/cm^2, which is twice larger than the output UCQC of the same FTNG without micro-structure. However, from the details of the current curve in Fig. 4c, it can be found that the pulses are messy and the peak values of most the pulses are small. This is because the adhesion between Nylon and PVDF films leads to difficulties in separating the positive and negative triboelectric charges, as shown in Fig. S3. To improve the performance of FTNG furtherly, some special films which have better elastic and tough behavior are needed. The film applied in FTNG should be thin enough to weaken the edging-effect and tensioned enough to counteract the electrostatic force.

Seven pieces of polyurethane (PU) film are cut from Okamoto condoms which's thickness is 0.01 mm. These PU films are stretched to ten times to their area and fixed in an annular PMMA support. Four pieces of PU films are coated 30 nm thickness Teflon film by magnetron sputtering and three pieces of PU films are coated 30 nm thickness SiO_2 film by magnetron sputtering. And then refer to the structure of the FTNG, a new FTNG with seven PU films and seven 180 μm high gaps is prepared. The photograph of the seven-layer PU structure is show in the inner figure in Fig. 4 d. The yellow part is annular support and the half-transparent part in the middle is the seven-layer PU structure. The output current and voltage are show in Fig. 4d and e. Due to the different lords in measuring process, the waveform of output current and voltage are different. From enlarged view of the currents in Fig. 4d, it can be found that the 14 current pulses, marked by red circles, are much clearer. So, this show that the PU films do not adhere to each other in the driving process. The total output charge per cycle of this FTNG can reach 454 nC. Since the effective area of the Al electrode is about 1.54 cm^2, an ultrahigh UCQC of 294 nC/cm^2 is calculated from the current curve, which is larger than the reported values of TENGs[35-39] and 1.18 times the record one[35](Fig. 4f). At last, the relationship curve of the UCQC of FTNGs with their number of gaps is shown in Fig. 4g.

Besides itself performance of TENG, the effective output is also determined by the external driving mode or working environment, especially, driving force, driving frequency, ambient humidity and so on. So, we studied the impact of driving force on the general TENG and FTNG. First, the FTNG with two 180 μm high gaps and a general TENG with no gaps are prepared. Using

View Article Online
DOI: 10.1039/D0EE00923A

a sliding table and a force sensor, the driving force on the TENG can be adjusted. And to avoid vibration, a soft sponge substrate is added behind the Al electrode, as shown in the inner figure in Fig. 5a. In fact, to ensure the synchronization between the linear motor and the tested TENGs, a soft substrate as the buffer layer is generally needed for TENGs. Driven under different forces, the half cycle currents of the general TENG and FTNG are measured and shown in Fig. 5a. The upper half of Fig. 5a is the output of the general TENG, the lower half is the output of FTNG, and the zoomed-in Fig. of the currents under 50 N force is shown in Fig. 5b. The two groups of currents both increase with the increase of driving force, and the currents of FTNG has one more splitting peak in half cycle than the general TENG. Analysing more detailed experimental data, the growth trends of UCQC are shown in Fig. 5c. For the FTNG, the increase of the output charge with the increase of force is quick at the first stage and then becomes slow, which is because too large force makes the polymer films adhere to each other and reduces the effective area of the films. Furthermore, if the soft substrate is changed into a tough one in the test process, the TENG will be vibrated strongly when the driving force is acted on the device. This is always inconvenient to analyse the experiment result, but it is much more efficient for energy harvesting and suitable for the practical situation. The half cycle currents of TENG and FTNG with tough substrates are shown in Fig. 5d and e. Due to the vibration, even the general TENG without multi-gap structure also generates several current pulses, about 12 pulses in half cycle. And the FTNG generates about 19 pulses in a half cycle. That means, even in the high frequency vibration conditions, the multi-gap structure can also multiply the frequency of the output current. Meanwhile, the UCQC of the general TENG and FTNG are shown in Fig. 5f, which depicts the excellent output performance of FTNG.

Next, to prove the effectiveness of frequency-multiplying solution through multi-gap structure design of friction layer for the high frequency energy harvesting, it is further applied in a sound wave harvesting TENG to fabricate a sound driven FTNG as shown in Fig. 6a. The device consists of two mesh substrates coated with Al film, a PVDF film with thickness of 5 μm, and a Nylon film with thickness of 5 μm. The polymer films and mesh substrates are separated by three spacers with the thickness of 180 μm. The compared device has the similar structure but only one PVDF film in the middle. To trigger them, a speaker is used to supply the sound wave, and the sound intensity and frequency are controlled by a program written with the LabView program. The output currents of these two devices driven at 100 dB and 150 Hz are shown in Fig. 6b. The black curve is the current of the general TENG with one PVDF film only, and the red curve is the current of the FTNG with both PVDF and Nylon film. From the enlarged view of the currents in Fig. 6c we can find that the red curve has one more pulse (marked by a red point) than the black one. Though the excess pulse is not split completely, it extends the width of the current pulse obviously. This will make the output charge increase. Fig. 6d shows the peak currents of the two devices at different frequencies with the sound intensity of 100 dB. Due to the additional one-layer Nylon film, the FTNG shows a higher current response and one more resonance frequency than the compared general TENG. These two resonance frequencies are 200 Hz and 450 Hz. The UCQC and total output charges in 48 s are shown in Fig. 6e and f. Besides the higher output charge quantity, the FTNG's output charge still displays a rising trend after the frequency of 350 Hz. However, for the compared device, its output charge declines sharply after the point of 350 Hz. These results demonstrate the frequency-multiplying technique with multi-gap structure friction layer can be used to every kind of TENGs.

Conclusions

In summary, a new frequency multiplying technique through designing the multi-gap structure friction layer has been successfully developed to gigantically increase the output performance of TENG. In the working process, these gaps in the friction layer supplies more contacting opportunities for the friction films with different electronegativity materials. The FTNG with three gaps in its friction layer creates 4 contacts between positive and negative layers in one cycle, three more contacts than the general TENG without gaps. This three-gap FTNG generate 6 output pulses and 15.6 nC/cm^2 UCQC, while a general compared TENG with no gaps in friction layer generated 2 pulses and 0.23 nC/cm^2 UCQC only. Besides, the effect of this multi-gap structure can work together with the other optimization routes, such as surface micro-structure building. A seven-gap structure can improve the UCQC from 0.23 nC/cm^2 to 47 nC/cm^2, and after combining with micro-structure modification on the friction layers' surfaces, the UCQC is improved to 98 nC/cm^2. Furthermore, more elastic PU film can prevent the adhesion of films in multi-gap structure and improve the UCQC to 294 nC/cm^2. At last, this new FTNG also shows an excellent performance in the sound wave harvesting.

Methods

Preparation of the PVA and PS solutions. 2.0 g PVA was mixed with 20.0 g deionized water in a 50 mL triangular flask. The solution was stirred at 80 °C for 3 h. 3.0 g PS was mixed with 8.0 g N, N-dimethyl formamide in a 50 mL triangular flask, then it was stirred for 3 h to ensure the dissolution of PS. All reagents were analytically pure and used without any further purification.

View Article Online
DOI: 10.1039/D0EE00021A

Fabrication of multi-gap layer. First, prepare a piece of PMMA substrate with side length of 3 cm. and a piece of corresponding size aluminum foil which was adhered on the surface of this substrate by the double sides tape. Then, several pieces of double sticky tape are used as spacers to bond aluminum foil and PS thin film which was prepared on a silicon wafer by spin coating method. The thickness of spacer can be adjusted by adjusting the layer number of the double sticky tape. And before being bonded, the PS thin film should be stripped from the silicon wafer and tensioned by a support. After that a PVDF thin film was prepared and bonded to the PS thin film in the same method.

Conflicts of interest

There are no conflicts to declare.

Acknowledgements

This study was supported by NSFC (No. 51603162, 81801847, 51903197), the Joint fund of Equipment pre-Research and Ministry of Education (NO. 6141A02022518), the Fundamental Research Funds for the Central Universities (No. JB191403, JB191401, lzujbky-2018-ot04).

Notes and references

‡ Footnotes relating to the main text should appear here. These might include comments relevant to but not central to the matter under discussion, limited experimental and spectral data, and crystallographic data.
§
§§
etc.

1. W. Ding, A. C. Wang, C. Wu, H. Guo and Z. L. Wang, *Advanced Materials Technologies*, 2018, **4**, 1800487.
2. X. Pu, H. Guo, J. Chen, X. Wang and Z. L. Wang, *Science Advances*, 2017, **3**, e1700694.
3. L. W. Zhong, *Acs Nano*, 2013, **7**, 9533.
4. Z. L. Wang, J. Chen and L. Lin, *Energy & Environmental Science*, 2015, **8**, 2250-2282.
5. Z. L. Wang, *Nano Energy*, 2018, **54**, 477-483.
6. F.-R. Fan, Z.-Q. Tian and Z. L. Wang, *Nano energy*, 2012, **1**, 328-334.
7. Z. Lin, B. Zhang, H. Zou, Z. Wu, H. Guo, Y. Zhang, J. Yang and Z. L. Wang, *Nano Energy*, 2020, **68**, 104378.
8. Y. Bai, L. Xu, C. He, L. Zhu, X. Yang, T. Jiang, J. Nie, W. Zhong and Z. L. Wang, *Nano Energy*, 2019, **66**, 104117.
9. X. Fan, J. Chen, J. Yang, P. Bai, Z. Li and Z. L. Wang, *ACS nano*, 2015, **9**, 4236-4243.
10. N. Cui, L. Gu, J. Liu, S. Bai, J. Qiu, J. Fu, X. Kou, H. Liu, Y. Qin and Z. L. Wang, *Nano Energy*, 2015, **15**, 321-328.
11. J. Liu, N. Cui, L. Gu, X. Chen, S. Bai, Y. Zheng, C. Hu and Y. Qin, *Nanoscale*, 2016, **8**, 4938-4944.
12. L. Gu, N. Cui, J. Liu, Y. Zheng, S. Bai and Y. Qin, *Nanoscale*, 2015, **7**, 18049-18053.
13. Y. Chen, Y. C. Wang, Y. Zhang, H. Zou, Z. Lin, G. Zhang, C. Zou and Z. L. Wang, *Advanced Energy Materials*, 2018, **8**, 1802159.
14. M. Xu, P. Wang, Y. C. Wang, S. L. Zhang, A. C. Wang, C. Zhang, Z. Wang, X. Pan and Z. L. Wang, *Advanced Energy Materials*, 2018, **8**, 1702432.
15. B. Zhang, L. Zhang, W. Deng, L. Jin, F. Chun, H. Pan, B. Gu, H. Zhang, Z. Lv and W. Yang, *ACS nano*, 2017, **11**, 7440-7446.
16. X. Wang, S. Niu, F. Yi, Y. Yin, C. Hao, K. Dai, Y. Zhang, Z. You and Z. L. Wang, *ACS nano*, 2017, **11**, 1728-1735.
17. R. Liu, X. Kuang, J. Deng, Y. C. Wang, A. C. Wang, W. Ding, Y. C. Lai, J. Chen, P. Wang and Z. Lin, *Advanced Materials*, 2018, **30**, 1705195.
18. Z. Lin, J. Chen, X. Li, Z. Zhou, K. Meng, W. Wei, J. Yang and Z. L. Wang, *ACS nano*, 2017, **11**, 8830-8837.
19. C. Dagdeviren, Z. Li and Z. L. Wang, *Annual review of biomedical engineering*, 2017, **19**, 85-108.
20. S. L. Zhang, Y. C. Lai, X. He, R. Liu, Y. Zi and Z. L. Wang, *Advanced Functional Materials*, 2017, **27**, 1606695.
21. N. Cui, J. Liu, Y. Lei, L. Gu, Q. Xu, S. Liu and Y. Qin, *ACS Applied Energy Materials*, 2018, **1**, 2891-2897.
22. Y. Zhong, H. Zhao, Y. Guo, P. Rui, S. Shi, W. Zhang, Y. Liao, P. Wang and Z. L. Wang, *Advanced Materials Technologies*, 2019, **4**, 1900741.
23. J. Chen, H. Guo, J. Zheng, Y. Huang, G. Liu, C. Hu and Z. L. Wang, *ACS nano*, 2016, **10**, 8104-8112.
24. S. Wang, X. Mu, X. Wang, A. Y. Gu, Z. L. Wang and Y. Yang, *ACS nano*, 2015, **9**, 9554-9563.
25. S. Xu, W. Ding, H. Guo, X. Wang and Z. L. Wang, *Advanced Energy Materials*, 2019, **9**, 1900772.
26. H. Qin, G. Cheng, Y. Zi, G. Gu, B. Zhang, W. Shang, F. Yang, J. Yang, Z. Du and Z. L. Wang, *Advanced Functional Materials*, 2018, **28**, 1805216.
27. J. Shao, T. Jiang, W. Tang, X. Chen, L. Xu and Z. L. Wang, *Nano Energy*, 2018, **51**, 688-697.
28. F. Xi, Y. Pang, W. Li, T. Jiang, L. Zhang, T. Guo, G. Liu, C. Zhang and Z. L. Wang, *Nano Energy*, 2017, **37**, 168-176.

29. Y. Zi, J. Wang, S. Wang, S. Li, Z. Wen, H. Guo and Z. L. Wang, *Nature communications*, 2016, **7**, 1-8.
30. C. Xu, A. C. Wang, H. Zou, B. Zhang, C. Zhang, Y. Zi, L. Pan, P. Wang, P. Feng and Z. Lin, *Advanced Materials*, 2018, **30**, 1803968.
31. C. Xu, Y. Zi, A. C. Wang, H. Zou, Y. Dai, X. He, P. Wang, Y. C. Wang, P. Feng and D. Li, *Advanced Materials*, 2018, **30**, 1706790.
32. C. K. Jeong, K. M. Baek, S. Niu, T. W. Nam, Y. H. Hur, D. Y. Park, G.-T. Hwang, M. Byun, Z. L. Wang and Y. S. Jung, *Nano Letters*, **14**, 7031-7038.
33. W. Tang, C. Zhang, C. B. Han and Z. L. Wang, *Advanced Functional Materials*, 2014, **24**, 6684-6690.
34. N. Cui, L. Gu, Y. Lei, J. Liu, Y. Qin, X. Ma, Y. Hao and Z. L. Wang, *ACS nano*, 2016, **10**, 6131-6138.
35. W. Liu, Z. Wang, G. Wang, G. Lin, J. Chen, X. Pu, Y. Xi, X. Wang, H. Guo, C. Hu and Z. L. Wang, *Nature communications*, 2019, **7**, 12744
36. Y. Zi, S. Niu, J. Wang, Z. Wen, W. Tang and Z. L. Wang, *Nature Communications*, 2015, **6**, 8376
37. J. Wang, C. Wu, Y. Dai, Z. Zhao, A. Wang, T. Zhang and Z. L. Wang, *Nature Communications*, 2017, **8**, 88.
38. C. Li, X. Qi, Z. Youbin, J. Xiaofeng and Q. Yong, *Nature Communications*, 2018, **9**,3773
39. J. Wang, S. Li, F. Yi, Y. Zi, J. Lin, X. Wang, Y. Xu and Z. L. Wang, *Nature Communications*, 2016, **7**, 12744.

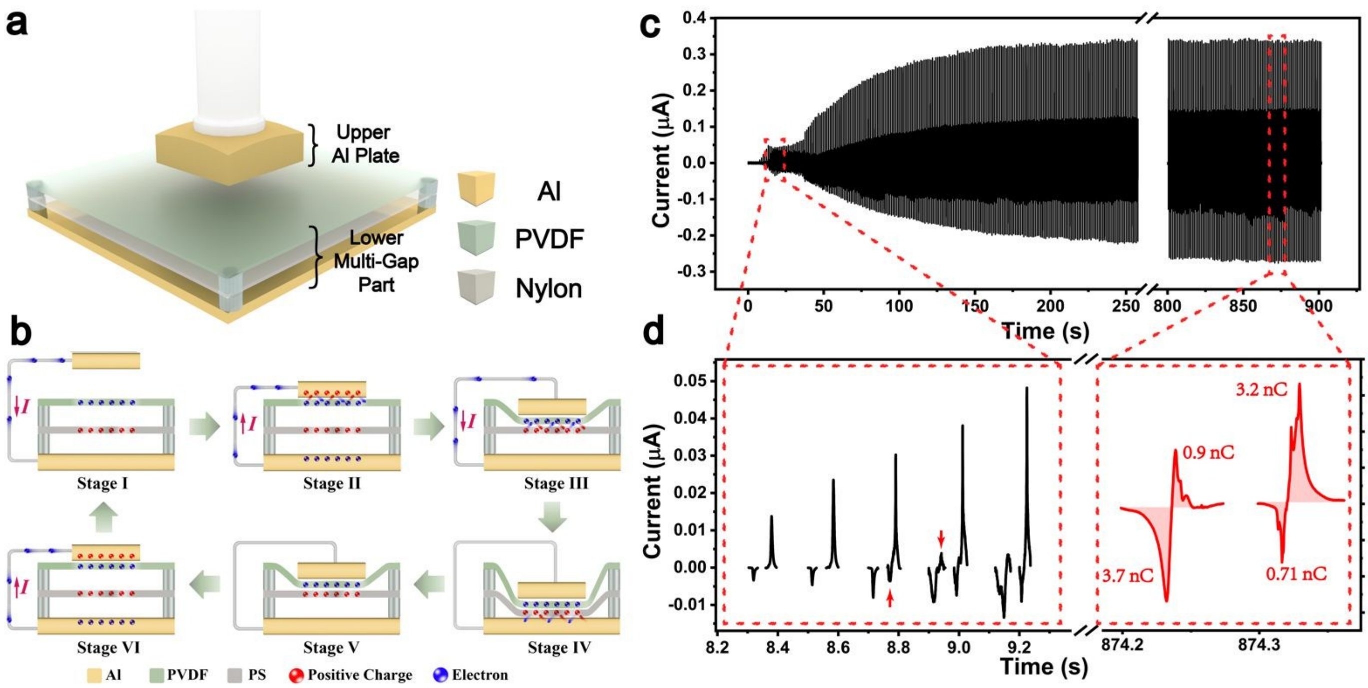

Fig. 1 (a) Schematic of the FTNG structure. (b) The basic working mechanism of a two-gap FTNG. (c) The output current of the two-gap FTNG. (d) The zoomed-in figures of the output currents.

View Article Online
DOI: 10.1039/D0EE00922A

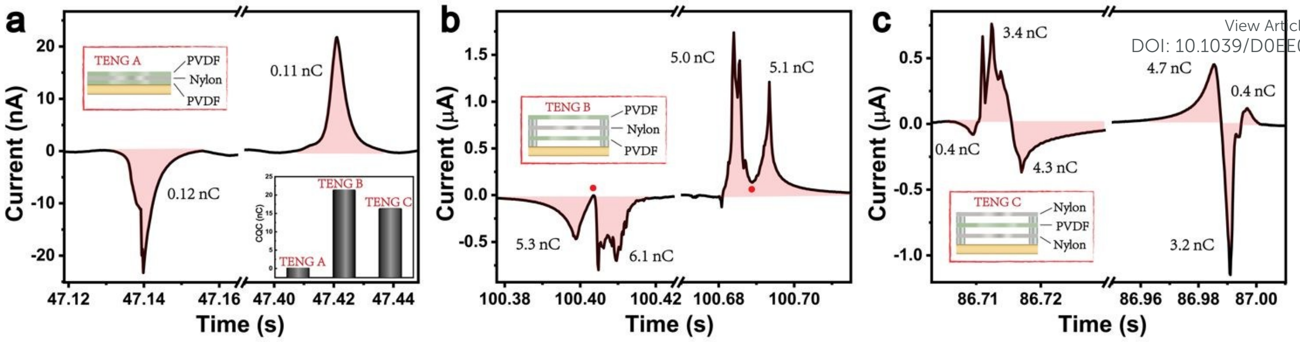

Fig. 2 (a) One cycle current output of TENG A with no gaps in its friction layer. (b) One cycle current output of TENG B. Its friction layer consists of PVDF film, Nylon film and PVDF film, and the height of the gaps is 180 μm. (c) One cycle current output of TENG C. Its friction layer consists of Nylon film, PVDF film and Nylon film, and the height of the gaps is 180 μm.

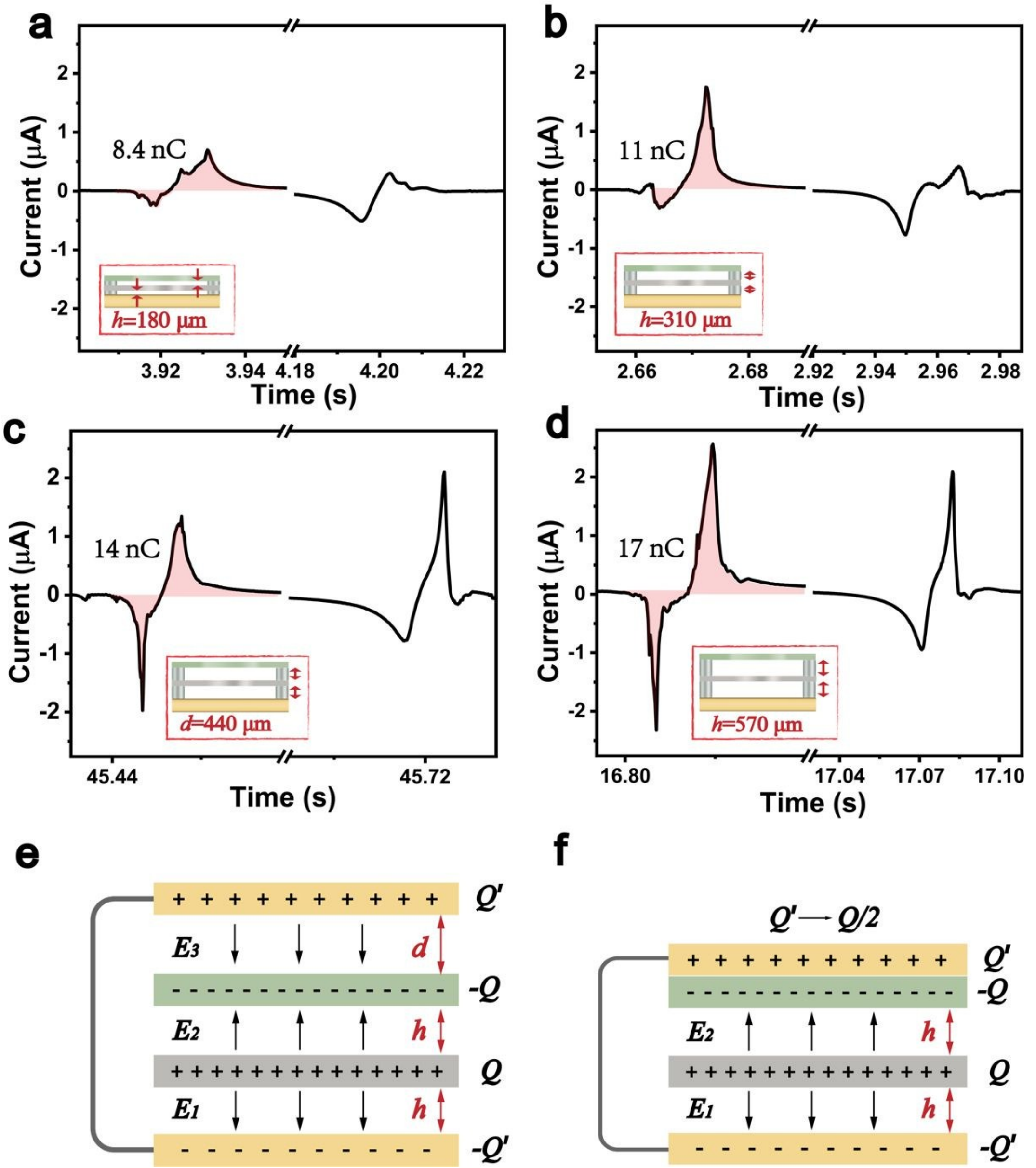

Fig. 3 (a-d) The current output of two-gap FTNGs which's gaps heights are 180 µm, 310 µm, 440 µm and 570 µm respectively. (e,f) The distribution of the induced charges in Al electrode at different states through theoretical calculation.

View Article Online
DOI: 10.1039/D0EE00922A

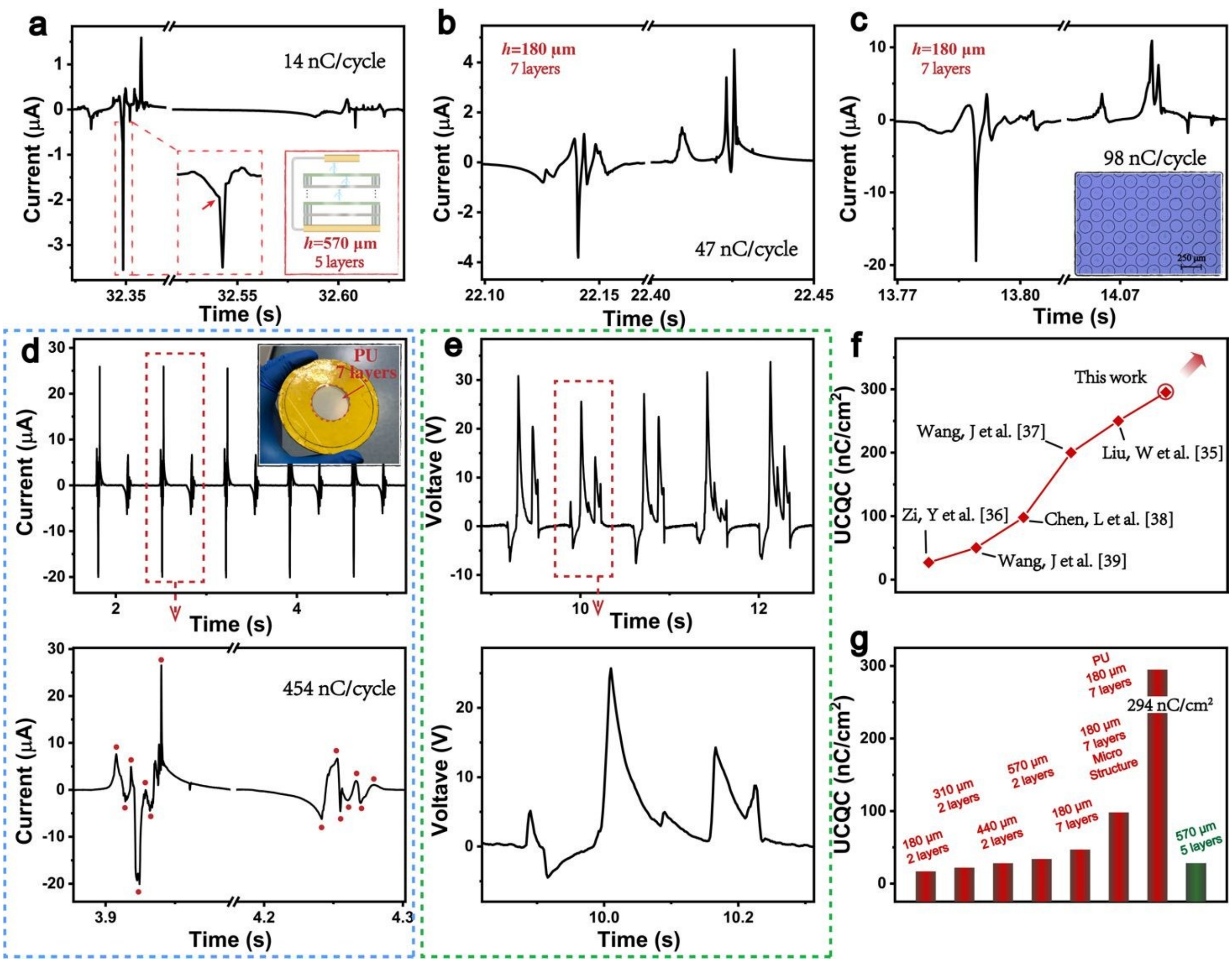

Fig. 4 (a) The current output of a five-gap FTNG with the gap height of 570 µm. In the test process the air discharges appear between the gaps frequently. (b) The current output of a FTNG with seven gaps. The height of each gap is 180 µm. (c) The current output of a seven-gap FTNG with micro-structure on the PVDF and Nylon films. The inset is the optical micrograph of the surface morphology of PVDF and Nylon film. (d) The current output and voltage output (e) of a seven-gap PU FTNG. (f) The UCQC of our seven-gap PU FTNG and selected representative TENGs. (i) The UCQC of FTNGs with different structures.

View Article Online
DOI: 10.1039/D0EE00922A

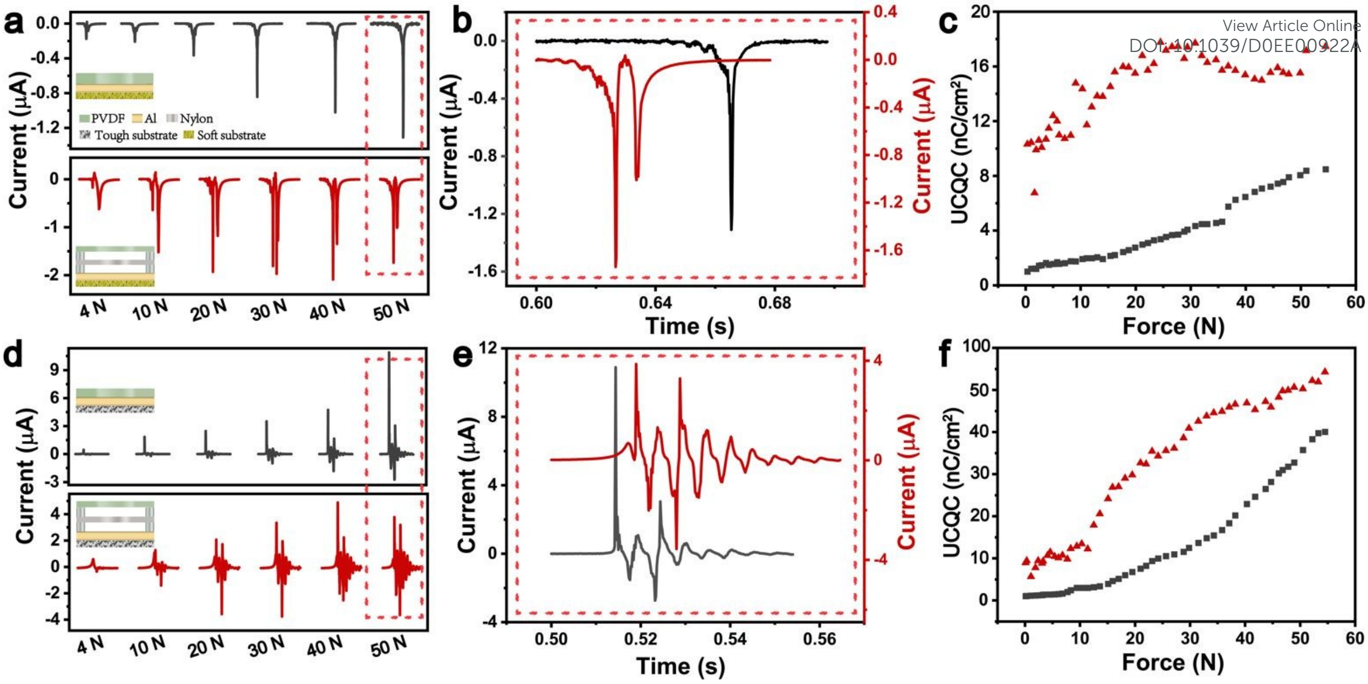

Fig. 5 (a) Comparison of output currents of TENG with (the red line) and without multi-gap structures (the black line) under different driven forces. These two TENGs both have a soft substrate behind the Al electrode. (b) The zoomed-in figures of the output currents in (a). (c) The increasing trends of the UCQC of TENG with soft substrates. (d) Comparison of output currents of TENGs with tough substrates. (e) The larger versions of the output currents in (d). (f) The increasing trends of the UCQC of TENGs with tough substrates.

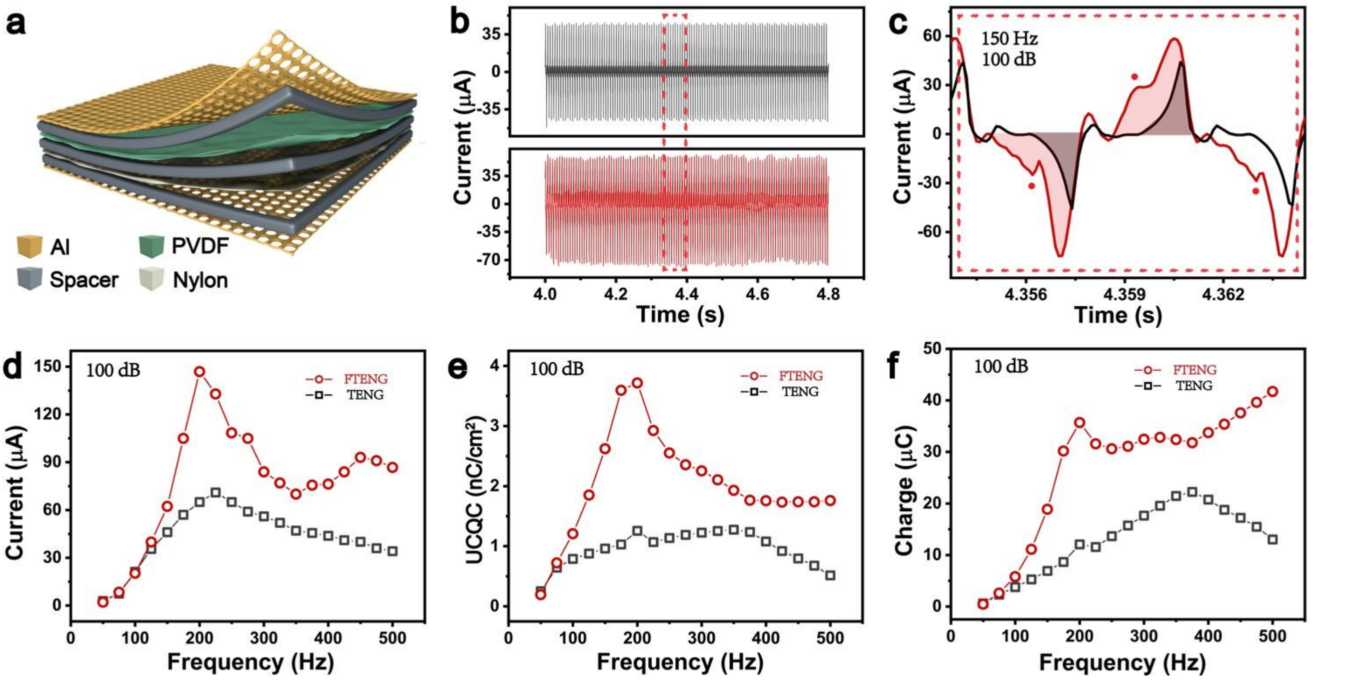

Fig. 6 (a) Schematic of the sound wave harvesting FTNG. (b) The black curve is the output currents of TENG with PVDF film in the middle. The red curve is the output currents of FTNG with PVDF and Nylon film in the middle. (c) The zoomed-in figure of the output currents in (b). The peak currents (d), UCQC (e), and output charge quantities in 48 s (f) of FTNG (red empty circle) and compared TENG (Black empty square) at different frequencies with the sound intensity of 100 dB.

View Article Online
DOI: 10.1039/D0EE00922A

Improving the output current and the output charge quantity continually is the main challenge in current triboelectric nanogenerator (TENG) studies. In principle, the output charge capability of TENG is strongly determined by the surface charge density of frictional layer and output current frequency. This work reports a multi-gap structure friction layer to greatly improve the charge output of TENG by increasing the surface charge density and output current frequency at the same time. This multi-gap structure consists of several staggered PVDF and Nylon films which have different electronegativity. In one working cycle, this structure can provide more contact times between PVDF and Nylon films. So more triboelectric electrons will transferred from Nylon to PVDF films. Meanwhile, every contact or separation of any two films will cause one current pulse in external circuit. The high surface charge density and more current pulses because of the contact and separation among many layers in one working cycle of TENG multiplies its output current and output charge quantity. Furthermore, the corresponding theoretical analysis and structure optimization of this multi-gap layer are made to maximize the output charge quantity of TENG. And one multi-gap structure TENG is developed for harvesting the high frequency sound.